Temperature Dependent Behavior of Thermal and Electrical Contacts during Resistance Spot Welding

E. Kim

Abstract

The thermal contact conductance at different temperatures and with different electrode forces and zinc coating morphology was measured by monitoring the infrared emissions from the one dimensionally simulated contact heat transfer experiments. The contact heat transfer coefficients were presented as a function of the harmonic mean temperature of the two contacting surfaces . Using these contact heat transfer coefficients and experimentally measured temperature profiles, the electrical contact resistivities both for the faying interface and electrode-workpiece interface were deduced from the numerical analyses of the one dimension simulation welding.

It was found that the average value of the contact heat transfer coefficients for the material with zinc coating (coating weight from 0 g/m^2 to 100 g/m^2) ranges from 0.05 $W/mm^2\,^oC$ to 2.0 $W/mm^2\,^oC$ in the temperature range above 50 ^oC harmonic mean temperature of the two contacting surfaces. The electrical contact resistivity deduced from the one dimension simulation welding and numerical analyses showed that the ratio of electrical contact resistivity at the faying interface to the electrical contact resistivity at the electrode interface is smaller than one for both bare steel and zinc coated steel.

Key Words : Resistance spot welding, Interface temperature, Temperature dependence, Thermal contact, Electrical contact, Contact heat transfer coefficient, Electrical contact resistivity, Zinc coated steel

1. Introduction

The most difficult part of understanding the science of the resistance spot welding process is the contact phenomenon. Basically the contact plays three different roles. As a mechanical contact it determines the current flow area and the mechanical constraint; as a electrical contact it produces heat and as a thermal contact it works as a barrier to heat flow. Due to the inherently complex nature of the interface, the contact phenomenon in resistance spot welding has been an obstacle to better understanding of the process.

Only very limited experimental studies have been made on the temperature dependency of contact properties[1-8]. Most of these studies were concentrated on the change of electrical contact resistivity as a function of static pressure or weld time. The difficulty lies in the fact that resistance spot welding is a transient process with a rapidly changing temperature field. Thus there are severe experimental difficulties. In this study, measurement of the thermal contact conductance at different temperatures and with different electrode forces and coating morphology are presented. And using the one dimensional numerical analysis, the electrical contact resistivity was also deduced from this thermal contact data and from the temperature fields measured in one dimensional simulation welding.

E. Kim : Senior researcher, Agency for Defense Development, Daejeon Korea
E-mail: keuiwhan@add.re.kr

2. Experimental procedures

2.1 Materials

The experiments were performed on low carbon steel of varying coating thickness and morphology. The electrode forces and materials are described in table 1.

2.2 One dimensional simulation welding

This test was used to determine the electrical and thermal contact properties of the work piece and the electrode. The characteristics of the electrical contact resistance were deduced from this experiment by comparing the results with the computer simulation which incorporates the interfacial heat transfer characteristics measured experimentally. The test setup was described in the reference 9[9].

Table 1 Experimental test materials

Symbol	Thickness (mm)	Coating	Coating Thickness (g/mm^2)	Electrode Force (lbs)
A40	0.8	galvannealed		500,650
G60	0.8	hot dip galvanized		500,650
E70	0.8	electro-galvanized	70/70	500,650
AMBR	0.8	electro-galvanized	0	500,650
AM35	0.8	electro-galvanized	35/35	500,650
AM68	0.8	electro-galvanized	68/68	500,650
AM100	0.8	electro-galvanized	100/100	500,650

2.3 Measurement of thermal contact conductance

The equipment for this test is shown in Fig. 1. In this Fig the length of the slender solid cylindrical electrode was 19 mm and the diameter was 4.8 mm. The electrode force was simulated by statically squeezing the two electrodes using a hydraulic press. The lower electrode was heated to the desired temperature using a radio frequency induction heater while the upper electrode was water cooled. The disk coupon was placed between two electrodes. The surface temperature was scanned along the electrode axis when a steady state temperature was established at the desired temperature. The scanning of temperature was performed using Thermovision system which monitors the infrared emission as described in the reference 9[9]. Due to the thermal expansion during heating process, the heating was performed under the electrode force less than the desired one. When the temperature of the hot electrode reached a little above the desired temperature, the electrode force was increased to the desired value while the heat was maintained. Due to the increased electrode force to the desired value the temperature field usually changed its distribution as soon as the electrode force was applied. A few seconds after the application of the desired electrode force the heating was halted and the data was recorded. By doing so, the effect of thermal expansion of the hot electrode was eliminated. The data were taken only during the heating process. The reason was to eliminate the effect of changes in the work piece surface. The thermal contact resistivity was calculated from this measured temperature profile. One scanning gives information from two locations, one for the upper interface and the other from the lower interface.

It should be noted that the upper interface has reversed temperature profiles compared to the profiles obtained in welding. During welding the work piece is always the hotter contacting member. In this experiment, particularly in the lower interface, the electrode is the hotter contacting member. This will cause some differences from the welding situation. However, due to the small size of the specimen, there is no alternative. This difference is considered later in the analysis of the measured data.

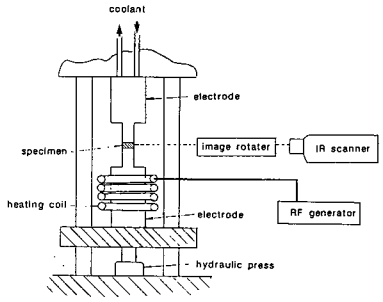

Fig. 1 Setup for heat transfer coefficient measurement

Since the temperature was read in a steady state mode and the electrode was a thin cylinder, the maximum temperature that the electrode could withstand was limited by the mechanical rigidity of the heated electrode. Due to this limit this experiment could be performed only up to 400 ^oC.

Using this method, the heat transfer coefficient across the electrode/work piece interface was estimated for various materials and various electrode forces.

3. One dimension numerical model

The one dimensional model is shown in Fig. 2 with boundary conditions. A four node isoparametric element was used for the body of the electrode and the work piece. At the electrode/work piece interface a two node interfacial element was employed. The model is axisymmetric with two elements in the radial direction. This is to check the validity of the solution by observing the temperature gradient in the radial direction. This also makes it easy to calculate the current density and the interfacial heat flux. Auniform current density distribution was used throughout the current path. Since the main purpose of this one dimensional model was to ascertain the characteristics of heat transfer and generation across the electrode interface, the length of the electrode was determined to be long enough to eliminate the effect of the water cooling. The actual

length of the cylindrical electrodes used in experimental tests was 1.9 cm. Due to the symmetry of the process, the model includes only one half of the system with insulated outer boundaries. Except for the electrical resistivity, the temperature dependence of the physical properties was collected from the published literature[10-13].

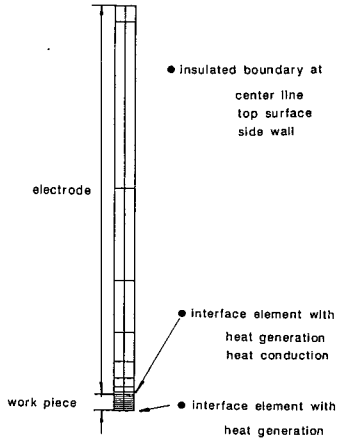

Fig. 2 Model for one dimensional simulation welding

This model was used to characterize the electrical properties of the interfaces. Using the temperature profiles measured during one dimensional simulation welding and the heat transfer coefficient across the interface, the electrical contact resistance across the contact interface was deduced.

4. Results and discussion

4.1 Contact heat transfer coefficient

Using the method of one dimensional simulation described in Fig. 1 the steady state temperature profiles across the electrode and the work piece were measured. The heat transfer coefficient, h_c was estimated from these temperature profiles. Fig. 3 shows a schematic of the temperature. In Fig. 4 typical temperature profile measured during experiment is shown. The thermal discontinuity can be seen at the interface. However as the interface temperature is not clear, the temperature profiles in each straight section were extended to find the cross point where the two extended profiles cross. The temperature at this point was measured as the interface temperature. Using these temperature profiles, the heat transfer coefficient at the contact interface was estimated. As stated previously this temperature profile was measured while steady state heat flow was maintained. Using the temperature notations in Fig. 3, the steady state heat flux balance across the specimen and the electrode can be written as follows.

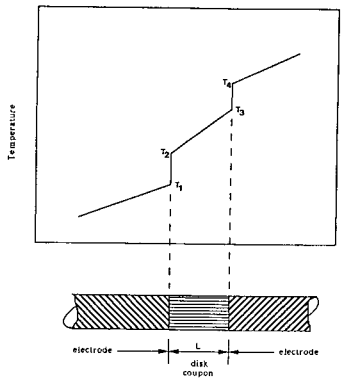

Fig. 3 Schematic temperature profile during the measurement of contact heat transfer coefficient

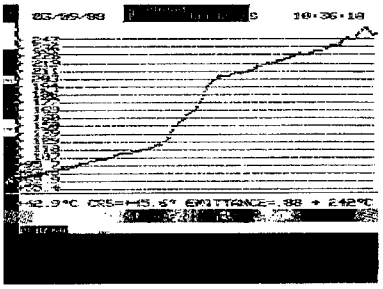

Fig. 4 Typical steady state temperature profile across the interface

$$h_c^{lower} = k\frac{(T_3 - T_2)}{L(T_2 - T_1)} \quad (1)$$

$$h_c^{upper} = k\frac{(T_3 - T_2)}{L(T_4 - T_3)} \quad (2)$$

Two heat transfer coefficients can be estimated from one measurement of the temperature profile, one from the upper interface, h_c^{upper}, and the other from the lower interface, h_c^{lower}. L is the disk coupon thickness and k is the thermal conductivity of the disc coupon.

The estimated heat transfer coefficients based on these measurements are shown in Fig. 5 to 15. In these fig. the harmonic mean of the contact temperature on the electrode side and on the work piece side was used as a temperature scale. The harmonic mean temperature (HMT) of temperature T_1 and T_2 is defined as

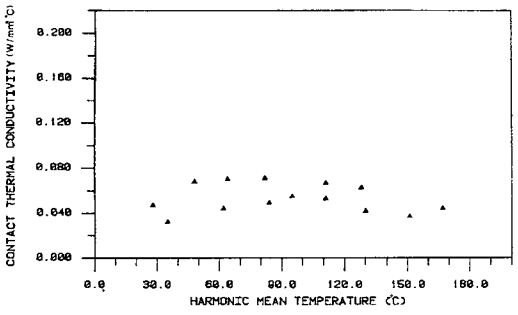

Fig. 5 Contact heat transfer coefficient of AMBR at 500 lbs electrode force

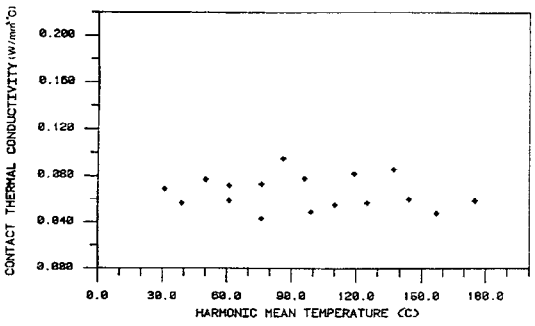

Fig. 6 Contact heat transfer coefficient of AM35 at 500 lbs electrode force

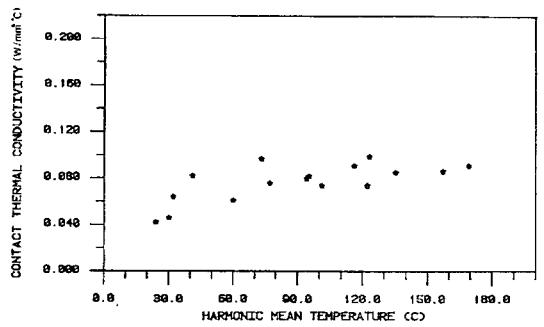

Fig. 7 Contact heat transfer coefficient of AM68 at 500 lbs electrode force

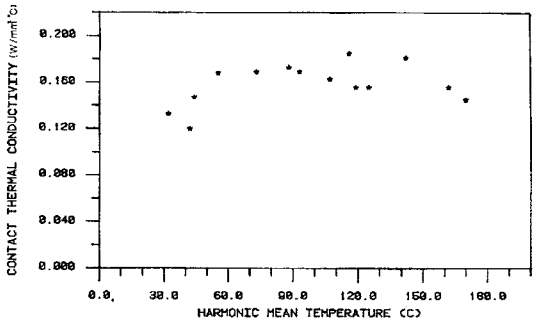

Fig. 8 Contact heat transfer coefficient of AM100 at 500 lbs electrode force

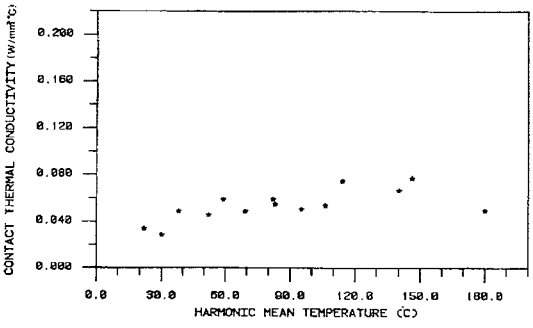

Fig. 9 Contact heat transfer coefficient of A40 at 500 lbs electrode force

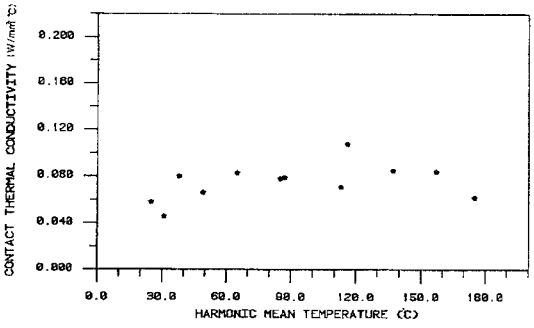

Fig. 10 Contact heat transfer coefficient of E70 at 500 lbs electrode force

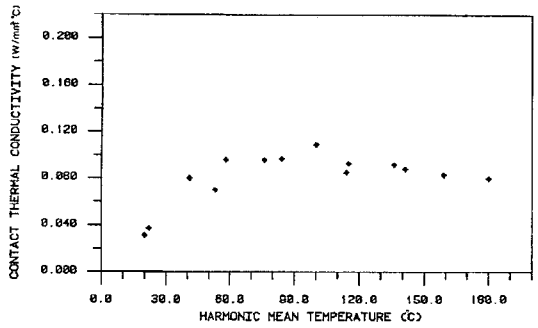

Fig. 11 Contact heat transfer coefficient of G60 at 500 lbs electrode force

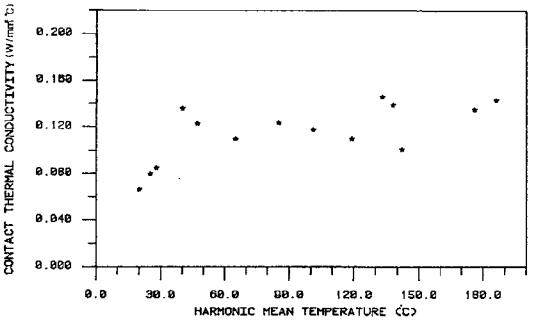

Fig. 12 Contact heat transfer coefficient of A40 at 650 lbs electrode force

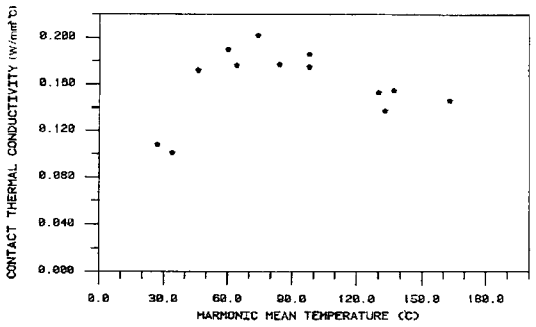

Fig. 13 Contact heat transfer coefficient of E70 at 650 lbs electrode force

$$T_{HMT} = \frac{T_1 T_2}{T_1 + T_2} \tag{3}$$

This parameter considers the effect of contact temperature differences between the electrode and the work piece. According to the theory of thermal contact resistances, the contact heat transfer coefficient is described as a function of the harmonic mean of the thermal conductivity of the contacting materials [14].

$$h_c = C_1 \frac{k_A \cdot k_B}{k_A + k_B} + C_2 \tag{4}$$

In this equation, k_A and k_B are the thermal conductivity of the contacting members and C_1 and C_2 are coefficients which are determined by variables such as the actual and the apparent contact area and the properties of the materials entrapped, if there are any, in the interface. Assuming a linear dependence of thermal conductivity with temperature, the harmonic mean of the contacting surface temperatures can be used to describe the contact heat transfer coefficient. This is particularly true in the temperature range experienced most often by the electrode/work piece interface i.e. from room temperature to about 600 ^oC.

From Fig. 5 to 15, it can be seen that the heat transfer coefficient increases with increasing temperature at lower temperatures. This is due to increases in the true contact area as the temperature increases. With further increases above 50 ^oC HMT it seems that there is no noticeable change in the contact heat transfer coefficient. It is likely that the maximum deformation of asperities occurs at this HMT due to the low mechanical strength of the electrodes or the zinc coating of the galvanized product. As the contact properties are generally determined by the softer contacting member this may be the same with the bare steel.

However, one thing that should be remembered in this analysis is that some part of the data (particularly the high temperature data) were measured with reversed temperature profiles as explained in experimental section. Even when the maximum interface temperature is about 400 ^oC, the specimen temperature is still lower than this temperature. As a consequence, even if differences in the mechanical behavior of the copper electrodes and the zinc are considered, there exists a possibility of underestimating the heat transfer coefficient. Considering the low melting temperature of zinc, 409 ^oC, it is obvious that the interface has not experienced zinc melting yet. The contact interface is still a solid to solid contact in this temperature range. This is another reason why the heat transfer coefficient data in Fig. 5 to 15 have flat plateau in the high temperature range.

The following equation for the contact thermal coefficient was derived by Mikic [15], for the case of plastic deformation of an interface.

$$h_c = 1.13 \frac{k \tan\theta}{\xi} \left(\frac{P}{H + P} \right)^{0.94} \tag{5}$$

In this equation k is the thermal conductivity, tan θ is

the mean absolute slope of an asperity profile, ξ is the standard deviation of the surface profile height, H is the microhardness and P is the normal pressure of the contact. This equation does not include any effect of temperature as a direct variable. However, it may be assumed that an increase of pressure has the same effect as an increase in temperature. This analogy is roughly correct due to the temperature dependence of the yield strength of the material. According to equation (5), the thermal contact coefficient should increase with temperature. In this experiment, the measured data did not show any conspicuous tendency to increase. Only a very slight increase was observed in Fig. 8, 9, 12 and 14. As explained previously, there is a tendency to underestimate the thermal contact coefficient in this experiment. Also the dominance of entrapped voids or contaminants on the contacting surface is possible. In any case, it is thought that the thermal contact coefficient should increase with temperature. Thus this should be considered in the numerical simulation. Another important feature of equation (5) is that the thermal contact coefficient has an asymptote as pressure increases (or as temperature increases).

Table 2 Contact heat transfer coefficient

Material	Thermal Contact Coefficient	
	@ 500 lbs	@ 650 lbs
AMBR	0.055 (0.013)	0.128 (0.009)
AM35	0.066 (0.015)	-
AM68	0.082 (0.013)	-
AM100	0.162 (0.015)	-
A40	0.058 (0.010)	0.126 (0.015)
E70	0.080 (0.013)	0.170 (0.020)
G60	0.089 (0.010)	0.182 (0.021)

units of W/mm^2 ^oC
numbers in parenthesis is a standard deviation

Average values of the heat transfer coefficient in the high temperature region are listed in Table 2 with standard deviations. For purposes of comparison, the average was taken excluding the values in the low temperature range. It can be seen that differences in zinc coating can cause marked differences in the interface heat transfer coefficient. As expected, the hard surface materials, such as bare steel and galvannealed steel, show low heat transfer coefficients compared to the soft surface materials such as hot dip galvanized or elctrogalvanized steel. It is also clear that the heat transfer coefficient increases as the amount of zinc on the surface increases. The range of contact heat transfer coefficient varies by 0.05 to 0.2 W/mm^2 ^oC in the temperature ranges and in the coating thickness ranges tested in this experiment. The changes in the coating thickness from 0 to 100 g/m^2 showed 4 times increase in the contact heat transfer coefficient.

The effect of electrode force can also be seen in the same table. Higher electrode forces result in higher heat transfer coefficients. The effect of electrode force is much more pronounced than that of coating morphology or that of the coating thickness. As the electrode force has a coupled effect on both the electrical contact resistivity and on the thermal contact heat transfer coefficient, the final effect of the electrode force on the lobe shape will be great.

The data presented thus far does not cover the entire temperature range experienced in the welding. In order for this data to be used in the numerical simulation it is necessary to characterize the contact heat transfer data more completely in the higher temperature range.

In the numerical simulation, the heat flux $\dot{Q}_c$, across the electrode interface is calculated using following equation,

$$\dot{Q}_c = h_c(T_{cb} - T_{ce}) \tag{6}$$

where, h_c : interface heat transfer coefficient
T_{cb} : interface temperature at work piece side
T_{ce} : interface temperature at electrode side

The heat transfer coefficient h_c in this equation was calculated as a function of the harmonic mean of the interface temperature T_{cb} and T_{ce}. Near 420 ^oC the zinc coating on the galvanized steel starts to melt and the contact will remain partially filled with molten zinc. From this temperature to the zinc vaporization temperature, about 910 ^oC, it may be assumed that the heat transfer coefficient remains constant. Thus one can see that there are thermal discontinuities throughout the welding process. This can be supported by the results of the experimentally measured dynamic electrical contact resistances[8-16].

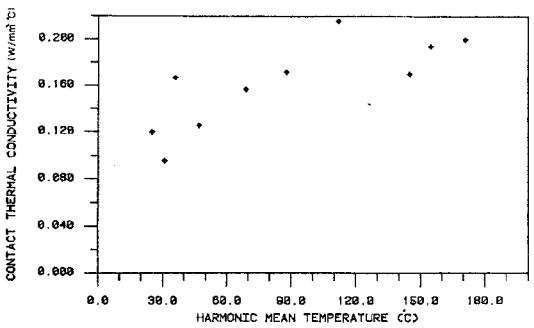

Fig. 14 Contact heat transfer coefficient of G60 at 650 lbs electrode force

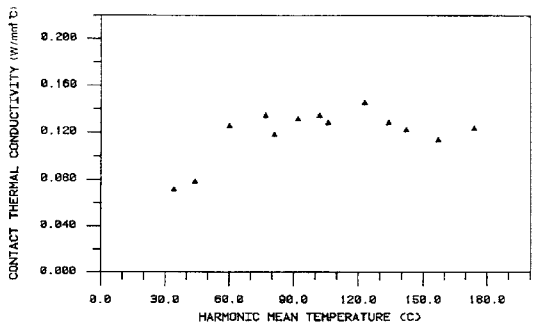

Fig. 15 Contact heat transfer coefficient of AMBR at 650 lbs electrode force

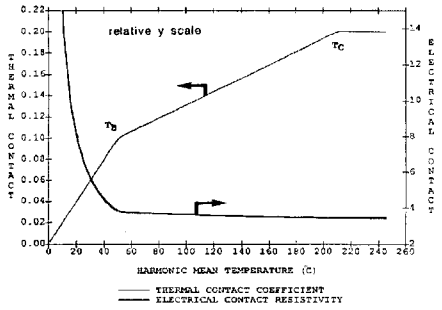

Fig. 16 Typical temperature dependence of the contact heat transfer coefficient and the electrical contact resistivity at the electrode interface

As was explained in the experimental section, the limit of experimental contact temperature measurement was approximately 400 ^{o}C in the electrode. However, as was presented in reference[9], the maximum electrode interface temperatures are scattered around 500 ^{o}C[9]. It is certain that the temperatures inside the electrode surface are higher than this surface value. Thus it is necessary to know the contact thermal conductivity above 400 ^{o}C . For this value one measurement was made with the AM100 specimen. While holding a low electrode force the specimen was heated until the zinc coating started to melt. Then the electrode force was increased up to the point where the hot electrode began to deform. The measured value was roughly 0.2 W/mm^2 ^{o}C. Thus this is a realistic value of the heat transfer coefficient above the zinc melting temperature for materials with free zinc on the surface. Due to the presence of molten zinc at the electrode interface at high temperatures, the heat transfer coefficient is assumed to remain constant at this value.

For the case of bare steel it was assumed that the coefficient gradually increases to the point where contact adhesion begins. The temperature of interface adhesion is known to be about 40 to 50% of the melting temperature[17]. Since the two contacting members have different material properties, it was assumed that the softer material governs the interface characteristics. For the present case, the melting temperature of the Cu-Cr electrode is about 1070 ^{o}C . Thus, 500 ^{o}C was chosen as a rough approximation of the adhesion temperature. Above this temperature the heat transfer coefficient was assumed to remain the same value as in the coated steel simulation.

The functional form of the contact thermal conductivity is defined in Fig. 16. In this fig. the harmonic mean temperature is again used. The entire temperature range is divided into three regions by T_B and T_C. The first region was chosen to be up to 50 ^{o}C of harmonic mean temperature (HMT), T_B. In Fig. 5 to 15 the experimental data shows a very rapid increase in thermal contact coefficient for each material below 50 ^{o}C HMT. It was assumed that the heat transfer coefficient at 50 ^{o}C HMT was equal to the average value shown in table 2. Following the observation of experimental data the heat transfer coefficients in this temperature range was assumed to change linearly with the heat transfer coefficient at 30 ^{o}C HMT is 60% that of 50 ^{o}C HMT. The second region was from 50 ^{o}C HMT to the zinc melting temperature or the interface adhesion temperature T_C in HMT. In this temperature region the coefficient was also assumed to increase linearly with temperature in HMT. In actual experiments only a very slight increase of the coefficient was observed. However as there exits a possibility of underestimation of coefficient in the high temperature range, it was simply assumed that the thermal contact coefficient increases from the average value given in Table 2 to a constant value of 0.2 W/mm^2 ^{o}C . For the melting temperature of zinc a HMT of 210 ^{o}C was used. For the interface adhesion temperature of the bare steel 250 ^{o}C HMT was used. The temperature for interface adhesion of a bare steel was also used for A40 galvannealed steel with the assumption that the mechanical property of this

material is close to the bare steel. To account for the varying amount of zinc on the surface, the upper limit of the second temperature region was assumed to vary from 210 ^oC to 250 ^oC in an inverse ratio to the amount of zinc. A third region was defined above this temperature T_C. It was assumed that the heat transfer coefficient remain constant in the third temperature region. The values for each material are tabulated in Table 3.

Table 3 Temperature dependence of heat transfer coefficient

Electrode Force (lbs)	Material	T_A 30℃ HMT	T_B 50℃ HMT	T_C (*)	(*) Temperature for T_C
500	AMBR	0.033	0.055	0.2	250
	AM35	0.040	0.066	0.2	235
	AM68	0.049	0.082	0.2	220
	AM100	0.097	0.162	0.2	210
650	A40	0.076	0.126	0.2	250
	E70	0.102	0.170	0.2	220
	G60	0.109	0.182	0.2	220

4.2 Electrical Contact Resistivity

Conventionally, the measurement of dynamic resistance in spot welding is performed as a function of time rather than as a function of temperature. In addition, the dynamic resistance is simply measured by monitoring the change in electrical potential across the entire contact interface. In this way the locally different contact resistance cannot be measured. Since the conventional method is time dependent there are difficulties in incorporating these data in the numerical simulation. Contact resistance data on a temperature base must be used in the numerical simulation. Therefore, in this research, the dynamic contact resistance was not directly measured. Instead, it was deduced by numerical simulation and the temperature profiles measured in the one dimensionally simulated spot welding experiments. In numerical simulation of one dimensional welding, the heat transfer coefficient of the electrode interface was incorporated as characterized in the previous section, leaving the electrical contact resistivity as an unknown variable.

The electrical contact properties were expressed in terms of electrical contact resistivity, σ_c, instead of the contact resistance, R_c, which is usually an integrated value over the total contact area. The electrical contact resistivity was defined as $\sigma_c = R_c \cdot A$. The dimension for this variable is ohm-unit area. By treating the contact electrical properties in this way it is possible to consider the effect of temperature on the electrical contact resistance. If the contact resistivity is multiplied by the current density the heat generation rate at the contact interface can be treated as a heat flux per unit area.

The contact resistivity was also treated as a temperature dependent quantity. According to the literature, the contact constriction resistivity, σ_c, can be related to the thermal contact conductivity as follows[17].

$$\sigma_c(T_\theta) = \frac{4}{h_c} L(T_\theta + T_0) \tag{7}$$

where, T_θ : temperature at the asperity contact (^oK)
T_0 : bulk temperature far away from contact (^oK)
L : Lorentz constant 2.4 x 10^{-8} $(V/^oK)^2$
σ_c : electrical contact resistivity (R_c = contacting area / σ_c)

This relationship was derived with the assumption that the Wiedemann-Franz law is valid and that the true contact is represented by a long narrow constriction. It can be roughly assumed that the spot welding process follows this equation in the early stages of welding, i.e. when the temperature is still low compared to the melting temperature of the contacting members. For example, assuming h_c to be roughly 0.1 $W/mm^2\,^oK$ as in Table 2, the value of σ_c at 100 ^oC becomes 0.64 $m\Omega - mm^2$

If the electrode diameter is 6.4 mm, the electrical contact resistance becomes 20 μΩ. This value is reasonably close to the published data[8]. However, one thing to be noted in this discussion is that there is a fundamental difference in electrical contact and thermal contact[17]. Films and other contaminants insulate more or less the electrical contact, but thermally they produce considerable short circuit paths for heat flow. Thus equation (7) is strictly valid only for clean metallic contacts in vacuum. In the actual spot welding process, the contacting surfaces are usually contaminated by foreign materials such as mill oil, oxide and dross pickup from the zinc bath and so forth. These contaminants will cause deviations of the contact characteristics from the ideal. Therefore, the direct estimation of electrical contact resistivity from equation (7) seems impossible even though the exact thermal contact coefficient data are given. For these reasons, only a functional relationship of equation (7) was used in this research with adjustable coefficients on one side of the equation (7).

The functional form of the contact resistivity for computer simulation can be derived from equation (7). Using an adjusting factor, F, this gives :

$$\sigma_c(T_{HMT}) = F \cdot \frac{(T_{HMT} + 146.5)}{h_c(T_{HMT})} \quad (8)$$

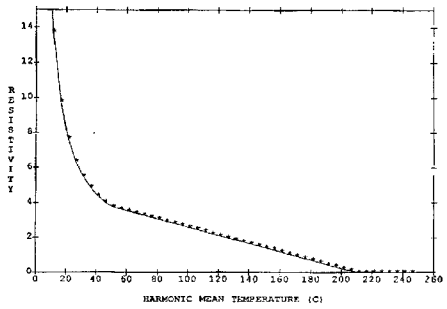

Fig. 17 Typical temperature dependence of electrical contact resistivity at the faying interface

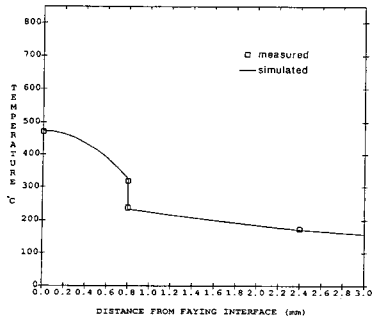

Fig. 18 Temperature profile for AM100 in 1-D simulation and the measured temperature

Two separate adjusting factors were used for each interface; one for the electrode interface, the other for the faying interface. This is necessary to account for the differences in the contact resistivity at the electrode interface and at the faying interface. Since the equation (7) is written in Kelvin scale it was changed to centigrade. The constant 146.5 in equation (8) is the room temperature in HMT replacing the temperature T_0 in equation (7). Considering the similarity between the electrical potential field and the temperature field, the harmonic mean temperature was also used as a temperature variable in the electrical contact resistance function. The final functional form of σ_c for the electrode interface is shown in Fig. 16. A linear functional form of h_c resulted in a hyperbolic functional form of σ_c.

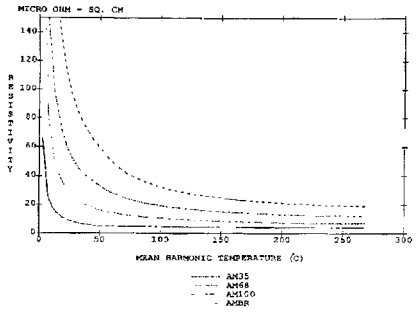

Fig. 19 Electrical contact resistivity at the electrode interface

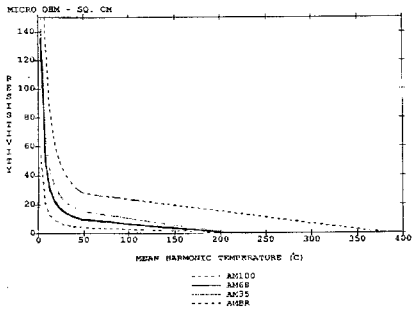

Fig. 20 Electrical contact resistivity at the faying interface

Fig. 17 shows the typical graph of contact resistivity at the faying interface. The contact resistivity at the faying interface was assumed to decay to zero as the temperature approaches the melting temperature of zinc (210 ^oC HMT). For bare steel, it was assumed that the contact resistivity at the faying interface decays to zero when the adhesion temperature of 765 ^oC (50% of melting temperature of steel, 383 ^oC HMT) is reached.

The contact resistivity was estimated by performing a one dimensional numerical simulation using the contact heat transfer coefficient data and the temperature fields as measured in the one dimensional simulation welding experiments. By changing the value of the adjusting factor, F, for both the electrode interface and the faying interface, the best combination of the contact resistivity curves which can reproduce the measured temperature profiles were determined. A sample of the predicted temperature is shown in Fig. 18 with experimentally measured temperatures. The final contact resistivity data deduced from these temperature profiles are shown in Fig. 19 and 20 for the electrode interface and for the faying interface respectively.

5. Conclusion

Based on the experiments and analyses, the followings can be presented as conclusions

1. The average value of the contact heat transfer coefficients for the material with zinc coating (coating weight from 0 g/m^2 to 100 g/m^2) ranges from 0.05 *W/mm^2 °C* to 2.0 *W/mm^2 °C* in the temperature range above 50 *°C* harmonic mean temperature of the two contacting surfaces.
2. The ratio of electrical contact resistivity at the faying interface to the electrical contact resistivity at the electrode interface is smaller than one for both bare steel and zinc coated steel.
3. The electrical contact resistivities at the faying interface decay to zero while the those at the electrode interface remains in the ranges from 5 μΩ-cm^2 to 20 μΩ-cm^2 depending on the amount of zinc coating.

References

1. D. K. Watney and G. L. Nagel: Forms of dynamic resistance curves generated during resistance spot welding, *IIW Doc.* No. III-823-85, IIW (1985)
2. W. F. Savage, E. F. Nippes and F. A. Wassell: Static contact resistance of series spot welds, *Welding Journal*, Nov. (1977), pp.365s-370s
3. W. F. Savage, E. F. Nippes and F. A. Wassel: Dynamic contact resistance of series spot welds, *Welding Journal*, Feb. (1978), pp.43s-50s
4. J. G. Kaiser, G. J. Dunn and T. W. Eagar: The effect of electrical resistance on nugget formation during spot welding, *Welding Journal*, June (1982), pp.167s-174s
5. S. A. Gedeon: Resistance spot welding of galvanized steel sheet, M. S. Thesis, Massachusetts Institute of Technology (1984)
6. S. Bhattacharya and D. R. Andrews: Resistance-weld quality monitoring, *Sheet Metal Industries*, July (1972), pp.460-466
7. G. L. Nagel and A. Lee: A new approach to spot weld feedback control, *SAE* 880371 (1988)
8. A. Lee and G. L. Nagel: Basic phenomena in resistance spot welding, *SAE* 880277 (1988)
9. E. W. Kim and T. W. Eagar: Measurement of transient temperature during resistance spot welding, *Welding Journal*, Aug. (1988), pp.303s-312s
10. Y. S. Touloukian et. al.: Thermophysical properties of matter, metallic elements and alloys, Plenum (1973)
11. Metals Handbook, American Society for Metals, 8th ed., Vol. 1 (1961)
12. Smithells: Metal reference book, 5th ed., Butterworths (1978)
13. D. D. Peckner and I. M. Bernstein: Handbook of stainless steel, McGraw-Hill Co. (1977)
14. J. P. Holman: Heat transfer, 4th ed. (1976)
15. B. B. Mikic: Thermal contact conductance; theoretical consideration, *Int. J. of Heat and Mass Transfer*, Vol. 17 (1974), pp.205-214
16. J. E. Gould and D. H. Cambell: The effect of conducting primers on the resistance spot weldability of automotive type sheet steels, *Sheet Metal Welding Conference III*, AWS, Oct. (1988)
17. R. Holm: Electrical contacts, 4th ed., Springer-Verlag New York Inc. (1967)